Journal of *Marine Science and Engineering*

MDPI

Article

3D Flooding Maps as Response to Tsunami Events: Applications in the Central Sicilian Channel (Southern Italy)

Salvatore Distefano *, Niccolò Baldassini, Viviana Barbagallo, Laura Borzì, Natale Maria D'Andrea, Salvatore Urso and Agata Di Stefano

Dipartimento di Scienze Biologiche, Geologiche ed Ambientali, Università Degli Studi di Catania, Corso Italia, 57, 95129 Catania, Italy

* Correspondence: salvatore.distefano@unict.it; Tel.: +39-09-5719-5724

Abstract: The assessment of the vulnerability of a site to tsunami events should take into consideration the geomorphological setting, which is strongly determined by the stratigraphic framework of the area. Lampedusa island is located in the central portion of the Sicilian Channel (Mediterranean Sea, Italy), where a significant incidence of tsunamis (with wave runup above 15 m) caused by earthquakes and submarine landslides has been historically documented. This work shows the geomorphological and stratigraphic differences between the western and south-eastern sectors of Lampedusa island. This update to the geological characterization of the island was used to create 3D flooding maps according to runup steps of 5 m, 10 m, and 15 m, thus showing a homogeneous involvement of the south-eastern sector of Lampedusa. Furthermore, our study aims to provide a geomorphological-stratigraphic base for a mathematical-statistical model to create coastal flooding maps due to tsunami waves. As such, this tool is useful for evaluation of strategic infrastructure for the security of the island and the improvement of risk management in civil protection.

Keywords: Lampedusa island; stratigraphic analysis; marine geology

Citation: Distefano, S.; Baldassini, N.; Barbagallo, V.; Borzì, L.; D'Andrea, N.M.; Urso, S.; Di Stefano, A. 3D Flooding Maps as Response to Tsunami Events: Applications in the Central Sicilian Channel (Southern Italy). *J. Mar. Sci. Eng.* **2022**, *10*, 1953. https://doi.org/10.3390/jmse10121953

Academic Editor: Efim Pelinovsky

Received: 25 October 2022
Accepted: 6 December 2022
Published: 8 December 2022

1. Introduction

Tsunamis are extremely devastating natural events for coastal areas. Tsunami hazards and flooding risks are much higher for low-lying coastal land. Cities and human activities are often on the coast and the attention to the exposure of people and human settlements to tsunami wave hazards has been increasing over the last decades [1], probably due to the catastrophic tsunami that occurred in North and Southeast Asia (December 2004, Sumatra, Indonesia).

Earthquakes, marine landslides, volcanic eruptions, and slumps are phenomena that can trigger tsunami waves. The Mediterranean Sea is one of the most active tectonic areas in history [2,3] and tsunami dynamics and effects on human life are well-documented within the Mediterranean countries [4–7]. The complex geodynamical setting and the tectonic evolution of the central and eastern Mediterranean areas are characterized by high seismic activity. Therefore, a large section of this paper is dedicated to the reconstruction of the historical geophysical archive of the eastern and central sectors of the Mediterranean Sea.

Low-lying and densely populated coastal areas are highly sensitive to large tsunami events, as shown by [8] in the two study cases they analyzed in the Island of Crete (Greece) and the Eastern Coast of Sicily (Italy). Refs. [9–12] show the fragility of the Ionian coast of Sicily (Italy) that is a densely populated area highly exposed to the tsunami hazard, and, in such parts, the flooding effects related to tsunami waves can be significant. Ref. [12] reconstructed the active tectonic structures and submarine landslides responsible for the 1743 earthquakes in southern Apulia. Ref. [13] shows evidence of the paleo tsunamis on the coastal zone of Cyprus. Ref. [14] analyzed the boulder accumulations related to extreme wave events on the eastern coast of Malta and [15] south-eastern coast of Cyprus.

An important parameter in the assessment of tsunami hazard is vulnerability, which is a function of a number of physical as well as social parameters that include, among others: distance from the shore, depth of flood water, construction standards of buildings, preparedness activities, socioeconomic status and means, level of understanding and hazard perception, and amount of warning and ability to move away from the flood zone. Thus, a tsunami vulnerability analysis should be developed with consideration of as many of these factors as possible in order to gain a more realistic picture of spatial and temporal patterns of physical and social vulnerability [16–21].

In particular, within the Sicily Channel (central Mediterranean) lies the Pelagian Archipelago, which comprises the islands of Lampedusa, Linosa, and Lampione [22–24]. Lampedusa is the largest and most populated of the Pelagian Islands, and tsunamis generated by the seismic activity of the central and eastern Mediterranean areas can hit its coasts causing huge damage. The region experiences problems of coastal erosion related to intense anthropic activity, as well as mass movement and land sliding, linked to the high variability of outcropping lithotypes and to the changeability of the coastal morphology. Furthermore, the geomorphological evolution is strongly conditioned by the presence of carbonate formations, where the development of the karst landforms is a typical dissolutive event as in other areas of south-eastern Sicily [25–27]. This work aims to provide a geomorphological-stratigraphic tool for creating tsunami marine ingression maps that could be realized by applying a mathematical-statistical model to Lampedusa island, which is particularly exposed to extreme events in the central Mediterranean Sea.

The geomorphological setting of the island is characterized by the Neogene-Quaternary depositional arrangement, which was determined by the new Lampedusa island stratigraphic analysis mainly performed on the eastern side outcrops. In fact, the significant differences between the western and eastern coastlines can be attributed to the presence of clear lithological variations between the two sectors of the island. The most cohesive sedimentary formations (bioclastic grainstones and biocalcarenites) are concentrated in the western portion, where high cliffs and regular coasts are especially widespread; conversely, a high lithological heterogeneity with the alternation of different lithotypes with variable cohesion (carbonate mudstones, marls, and alluvial deposits) is concentrated in the south-east area where lower and more irregular beaches develop.

Historical Geophysical Framework in the Mediterranean Area

Tsunami events have often caused serious damage within the Mediterranean Sea and most of these events are well known from historical records. The sources that can trigger tsunamis are different. The waves could be related to strong winds and marine storms but also by large submarine landslides or volcanic activity [28–30], and the Mediterranean Sea is one of the most active tectonic areas, in which earthquakes and related triggered tsunamis pose a significant risk.

From 2300 BC to the present day at least 290 tsunamis have occurred in the Mediterranean [31]. To date, the geological evidence of tsunamis and floods that occurred in prehistoric times is still identifiable. The Ionian coast and the Sicily Channel have been hit by at least 10 tsunamis in the last 2000 years, and prehistoric geological evidence reports the occurrence of paleo floods around 2300 BC and 1635 BC, 975–800 BC, 800–600 BC, and 600–400 BC [32]. Table 1 shows the main tsunamigenic events in the central-eastern Mediterranean Sea, with the relative maximum runup value.

In historical times, several tsunamis generated by earthquakes hit the south-eastern coast of Sicily, as in 1169 AD, 1693 AD, and 1908 AD [46]. Such events may be of sufficient size as to propagate, as previously happened, in the direction of the Sicily Channel, affecting the Maltese archipelago and the Pelagie Islands. There are now numerous published data and related numerical modeling that demonstrate that the seismogenic source of events of this type can be located in the Ionian offshore (the Malta Escarpment [47–50]), in the Strait of Messina, in the Graben of Linosa [51], and in the area of the Hellenic arc [52,53]. The Ionian coast of Sicily and the Sicily Channel, the Maltese Archipelago, and the Pelagie

Islands are, therefore, places not at all alien to the risk of large earthquakes followed by devastating tsunamis, such as the events of 1169 AD, 1693 AD, and 1908 AD.

Table 1. Main tsunamigenic events in the central-eastern Mediterranean Sea (Euro-Mediterranean Tsunami Catalogue—EMTC). The numbers in the first column are identifiable in Figure 1.

	Date	Seismic Source	Hit Localities/Areas	*Runup* (m)	Magnitude	Inundation (m)	References
1	21 July 365	Crete-Gortyna	Sicily and many other islands	***2***	8–8.5	1200	[33,34]
2	5–6 February 1783	Southern Calabria	Torre Faro, Messina, Scilla, and Southern Calabria	***9***	7.1	200	[35,36]
3	2 June 1866	Crete	Eastern coast of Kythira Island	***8***	–	–	[37–39]
4	28 December 1908	Messina Straits	Eastern Sicilian coast and Southern Calabria	***1–3***	7.1	380	[40–42]
5	3 July 1916	Stromboli	Aeolian Islands	***10***	5–6	20	[43]
6	9 July 1956	South Aegean Sea	Amorgos	***25***	7.5	80–100	[44,45]

Concerning the recent tsunamigenic seismic activity of the Sicily Channel, the first field research was performed in the Mediterranean Sea between the end of the 20th century and the beginning of the 21st century [54]: along the coast of central Greece [55] and of Southern Italy [56,57], along the coast of Cyprus and Crete [58–60], and along the coast of Algeria [61].

Owing to the wealth of historical and geological data collected over the last decades on the effects of seismicity in the Mediterranean, various databases were created to map the most vulnerable sectors to the occurrence of earthquakes and consequent tsunami floods, with the aim of cataloging the distribution and runups that have occurred and that could occur (Figure 1).

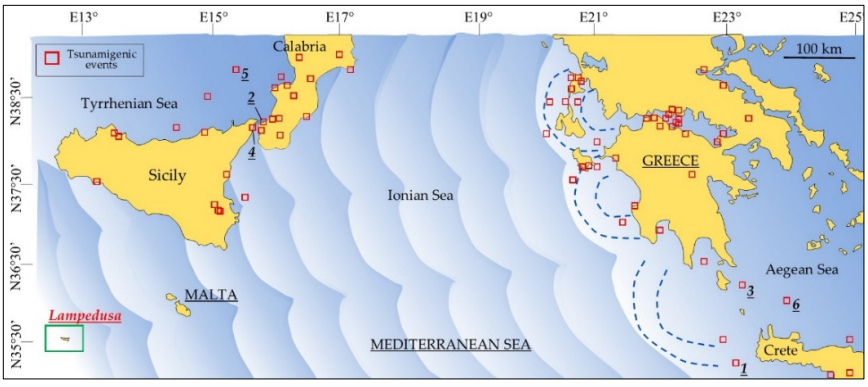

Figure 1. Localization of the main tsunamigenic events of the last 1800 years with a schematic representation of the direction of the main wave fronts of expected tsunami propagation in the Mediterranean Sea (Euro-Mediterranean Tsunami Catalogue—EMTC). In the green box is the study area. Numbered events refer to Table 1. The wavy trend of the contours represents the direction of a possible wave-front propagation in the eastern Mediterranean Sea.

The accumulation of large boulders related to waves generated by either tsunamis or extreme storm events has been observed in different areas of the Mediterranean region. Heavy storms are quite common in the Mediterranean Sea and often originate from the NW and NW winds. To verify whether the detachment of the boulders is due to tsunami events

or storm waves generated in the area, a hydrodynamic approach can be applied ([14] and references therein). The application of hydrodynamic equations, in addition to radiocarbon dating [14], demonstrated how 10% of a population of boulders sampled in Malta can be associated with tsunami waves, and according to radiocarbon analysis, the age of the 5% of the boulders is of such age as to be associated with a recognized tsunami-related event. Even assuming that the hydrodynamic approach is not sufficient to distinguish between storm and tsunami waves as a stand-alone method, these equations are, however, useful to hypothesize potentially reachable runups by waves necessary for the movement of boulders found in the archipelagos of the Sicily Channel.

Even considering the uncertainties exposed by [14], it is still valid that extreme storms and tsunamis have occurred generating runup that reached levels between 13.35 and 14 m. Moreover, in some cases, the analyzed values obtained for the runup of tsunami waves are comparable to those observed during the 1908 earthquake [62,63], as well as those obtained by [64] for tsunamis generated by earthquakes both in eastern Sicily and in the western Hellenic arc.

The Mediterranean area can be divided into two macro areas. The first is the Eastern Mediterranean Basin where the Hellenic arc is the major geotectonic structure dominating the eastern Mediterranean basin and producing large earthquakes and tsunamis. The second is the Western Mediterranean Basin, where tsunamis were reported in North Algeria to have been caused by strong earthquakes occurring on AD 2 January 1365; 6 May 1773; 21–22 August 1856; 9 September 1954; and 10 October 1980 [65]. Ref. [66] suggests that the location of most of these earthquakes on land in North Algeria triggered submarine landslides that generated powerful turbidity currents. However, the 21 May 2003 small-to-moderate tsunami produced by the Mw 6.8 Boumerdes–Zemmouri (Algeria) earthquake in the continental margin of Algeria was attributed to a thrust co-seismic faulting.

Field observations performed after modern tsunamis, particularly the 2004 Indian Ocean and the 2011 northeast Japan tsunamis, have shown that strong tsunamis are capable of causing significant geomorphological changes [65], which may include beach erosion, disruption of sand barriers and dune systems, and also erosional escarpments and large scars [67]. In the Mediterranean region, the creation of washover fans, landward oriented within lagoons or coastal lakes, has been interpreted as due to the action of tsunamis [57,65,68].

Important geomorphological variations are also recorded in offshore areas in proximity of numerous coastlines of the Mediterranean area. The authors in [52,56] note that both inflow (landward) and outflow (seaward) caused intense erosion, sediment transport, and deposition. Moreover, the amount of sediment reworked, transported, and deposited offshore by the outflow was probably larger than the volume deposited inland during the 2004 Indian Ocean tsunami [65,69]. These recent findings show that offshore there is a higher potential for recording "anomalous" events, that is, tsunamis but also earthquake-triggered mass transport deposits, with respect to the coastal environments that experience intermittent and variable deposition/erosion as well as important human disturbance [65].

2. Geological Setting of the Sicily Channel, Italy

The Sicily Channel is a complex geodynamic sector (Figure 2) where extensional tectonics interact with the Africa-Europe convergence [70–73]. Specifically, the area has suffered two main rifting phases [74,75]. The youngest rifting phase occurred since the late Miocene and controlled the evolution of the sedimentary basin where the deposits characterizing Lampedusa island formed. During this rifting event, the extensional activity mainly develops through a set of WNW–ESE and NW–SE trending normal faults, dissecting a shallow-water continental shelf (Malta, Tunisia, and Adventure plateaus), and giving rise to a zone of stretched lithosphere between Sicily and Tunisia [76,77]) reported as the Sicily Channel Rift Zone (SCRZ) [78,79]. Concerning the Neogene to Quaternary structural evolution of the Lampedusa offshore, ref. [80] show that it was largely affected by extensional tectonics, which produced differential uplifted and subsided areas.

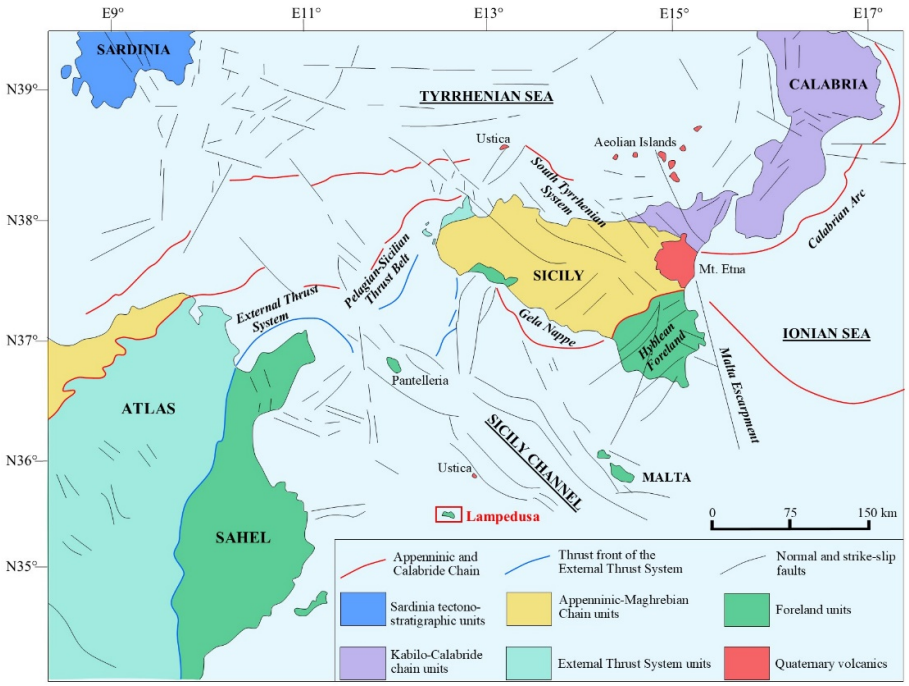

Figure 2. Geological setting of the Sicily Channel.

Lampedusa lies on the northern edge of the Tunisian continental shelf and represents a small emerged portion of the Pelagian Block [71,81–83]. The Pelagian Block outcrops in south-eastern Sicily (Hyblean foreland) and the onshore and offshore Neogene-Quaternary geodynamic evolution has been widely studied [48,84–86]. The Hyblean Plateau represents the foreland domain of the Apennine-Maghrebine fold and thrust belt in Sicily [87–94] associated with the Mesozoic collision between African and European plates [95].

2.1. Stratigraphic Setting of Lampedusa Island

The sedimentary succession cropping out in Lampedusa island is late Miocene to early Pleistocene in age, and it is unconformably covered by Holocene deposits [23,24] (Figure 3).

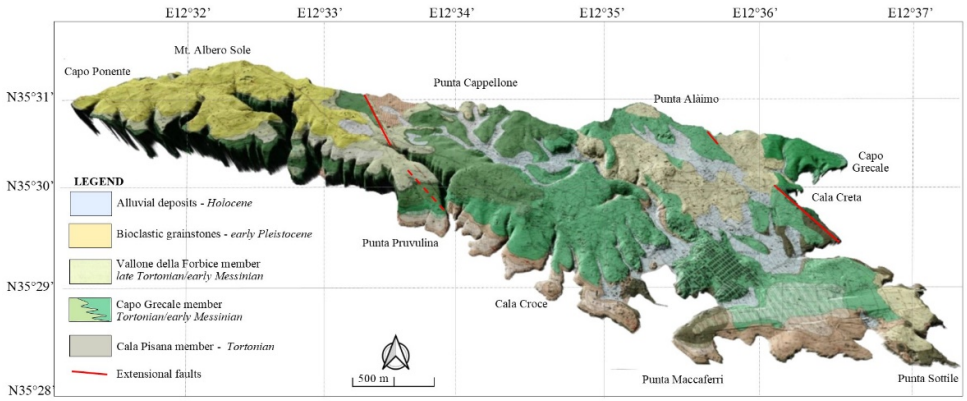

Figure 3. Geological map of Lampedusa island.

The oldest rocks belong to the Lampedusa Formation, which is divided into the Cala Pisana, Capo Grecale, and Vallone della Forbice members.

2.1.1. The Cala Pisana Member (Mb)

The attributed age for the Cala Pisana Mb is Tortonian (Late Miocene), according to [15], which crops out only in the eastern and southern parts of the island. The member

is subdivided into the following two intervals, which are at least partially heterotopic (Figure 4):

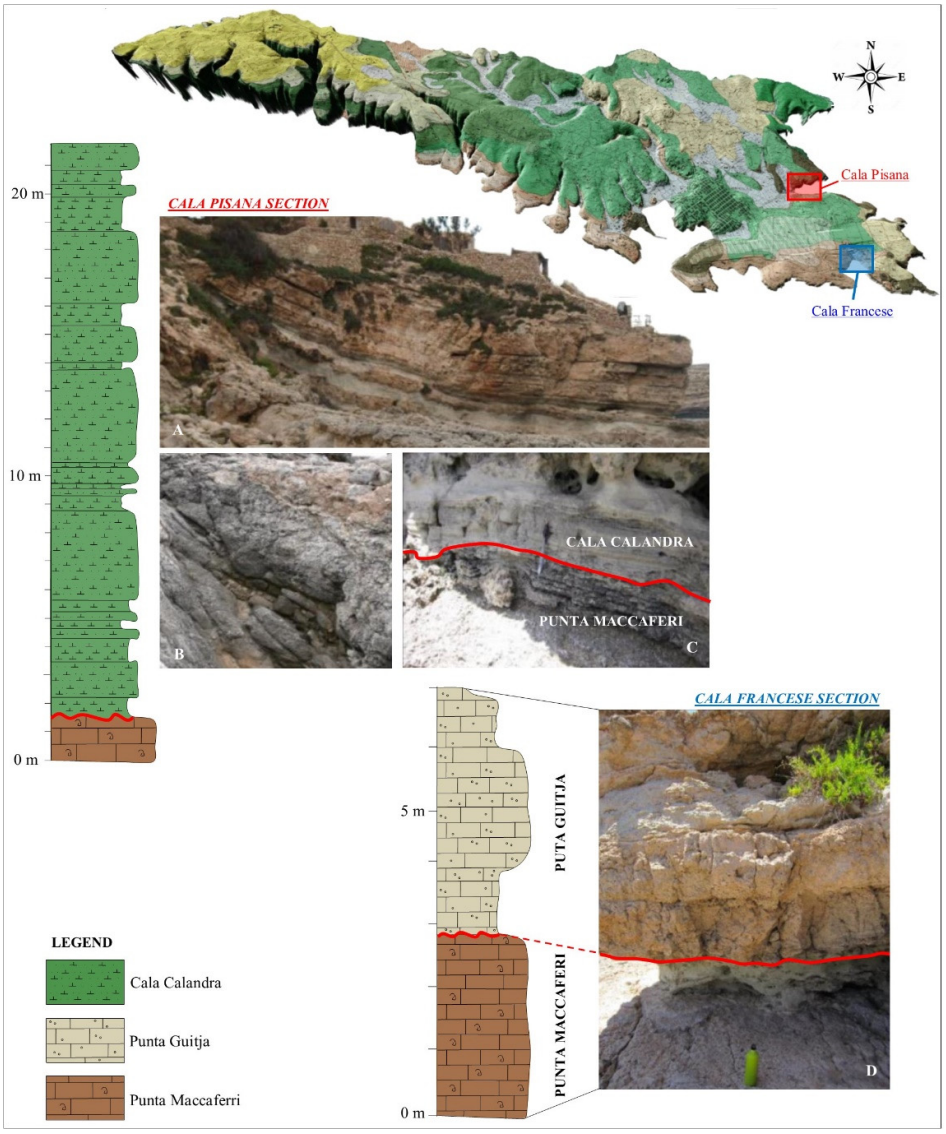

Figure 4. Lithologic log of the Cala Pisana and Cala Francese sections. (**A**) Panoramic view of the Cala Pisana outcrop. (**B**) Punta Maccaferri Beds. (**C**) Detailed view of the sharp contact between the Punta Maccaferri and Cala Calandra Beds. (**D**) Detailed view of the Punta Maccaferri Beds–Punta Guitja Beds transition.

(a) Punta Maccaferri Beds: biomicrites rich in Porites, coralline algae (Halimeda), serpulids, gastropods (Arca and Conus), and sponges (Entobia) followed by a few meters of grey wackestones and by Porites biostromes. These deposits are typical of a reef environment and show a maximum thickness of about 30 m in the Capo Grecale area, along the north-eastern coast.

(b) Punta Guitja Beds: oolitic limestones and rhodolitic algal levels with abundant bioturbations, showing a maximum thickness of about 6 m. These deposits, cropping out about 5 m a.s.l., are typical of a fore-reef depositional (10–15 m deep) environment that deepens westwards.

2.1.2. The Capo Grecale Mb

The Capo Grecale Mb extensively crops out throughout the island. It unconformably lies above the beds of the Cala Pisana Mb in the central and eastern part of the island while, in the western part, it crops out along the coast and characterizes the deepest parts of the numerous fluvial incisions (Vallone dell'Acqua, Vallone Profondo, Vallone della Forbice, and other smaller valleys). Ref. [22] ascribed this member to the Tortonian to early Messinian time interval, and recognized two different intervals well represented on the island, namely (Figure 5):

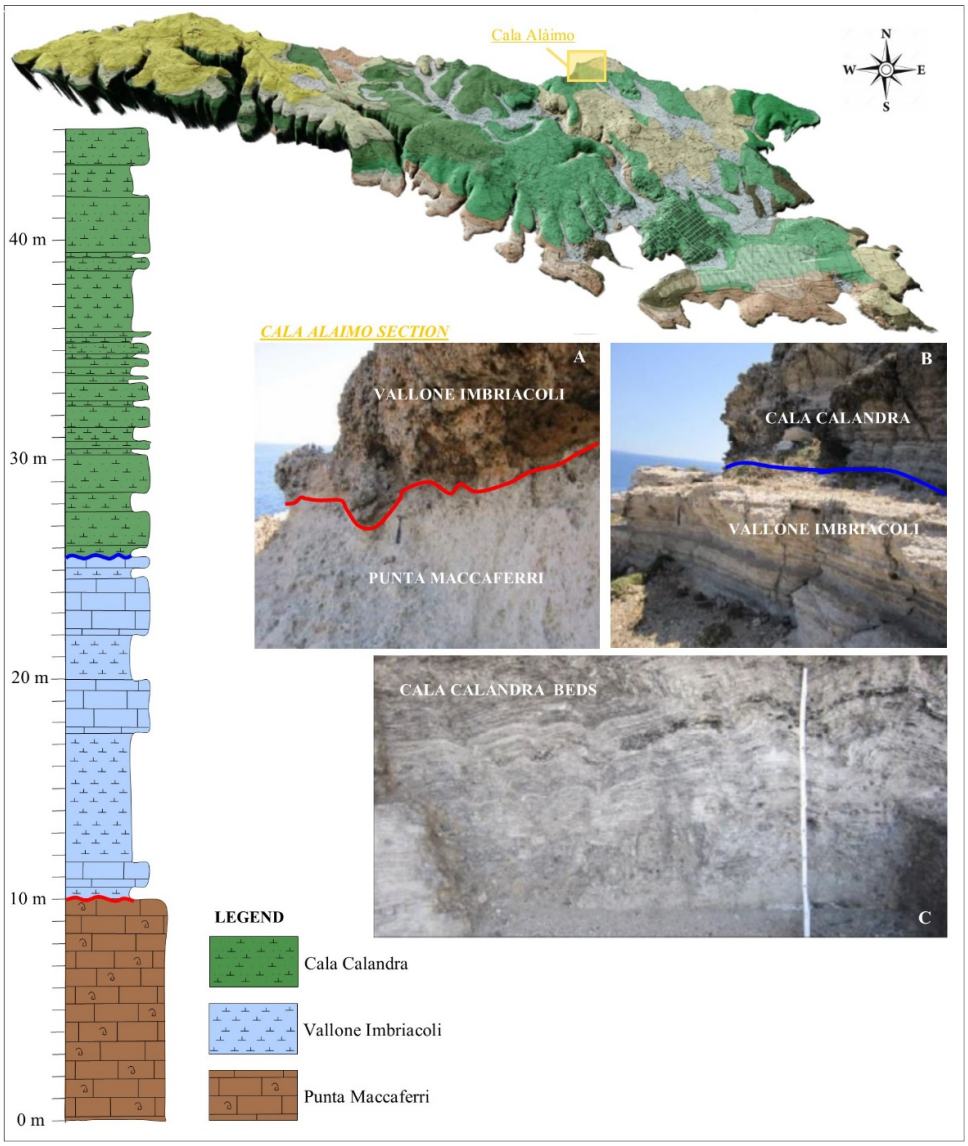

Figure 5. Lithologic log of the Cala Alaimo section. (**A**) The Vallone Imbriacoli Beds-Punta Meccaferri Beds contact. (**B**) The Cala Calandra Beds–Vallone Imbriacoli Beds contact. (**C**) Detailed view of the laminates of the Cala Calandra Beds.

(a) Vallone Imbriacoli Beds: carbonate mudstones and wackestones (maximum thickness 18 m) yellowish-white in color, with abundant pectinids, oysters, echinoids, and bryozoans. Benthic foraminifera, such as *Ammonia beccarii* and *Elphidium crispum*, are also widely distributed within these deposits. These beds widely occur in the cliffs along the western and northern coast of the island where they transitionally lie above the Punta Guitja Beds. Conversely, they unconformably lie above the Punta Maccaferri Beds between Cala Pisana and Cala Creta, along the eastern coast.

(b) Cala Calandra Beds: the first 50 cm are represented by a marly lithotype topped by a slumped bed (3 m thick) consisting of cream micrites and wackestones. The uppermost part of the bed is characterized by thinly layered biocalcarenites of pale brown color. The unit crops out only in the eastern part of the island, immediately east of the Cala Creta Fault, and shows a syntectonic development [22].

2.1.3. The Vallone Della Forbice Mb

The Vallone della Forbice Mb crops out in the western and northern part of the island and consists of about 60 m of partly dolomitized biocalcarenites, yellowish to pale grey in color, deposited between late Tortonian and early Messinian [22]. In the middle part of the unit, the carbonatic Lumachelle Bed occurs. The upper part of the member is characterized by a few meters of dolomite laminites and thinly laminated stromatolites. The unit is characterized by the presence of common benthic foraminifera, coralline algae (Halimeda), mollusks, echinoids, corals, and bryozoans.

2.1.4. Pleistocene and Holocene Deposits

A wide stratigraphic gap separates the Pleistocene and Holocene deposits from those belonging to the three late Miocene members. The younger lithotypes consist of:

(a) White to pink bioclastic grainstones attributed to the early Pleistocene by [22] and mostly distributed in the western part of the island.

(b) Tyrrhenian wave-cut platforms, with abundant fossils of Strombus bubonius cropping out at 8.60 m above sea level [67]. This elevation is consistent with that recognized for the Tyrrhenian wave-cut platforms in the Mediterranean area (+7 m; $\pm$ 1 m above the present sea level), and allows to recognize a substantial tectonic stability for the island of Lampedusa in the last 125,000 years.

(c) Bioclastic grainstones with aeolian dune bedding showing a small amount of quartz that has been transported by winds from the Sahara during the late Pleistocene (Giraudi, 2004 [47]).

(d) Carbonate lithoclastic breccias characterized by "terra rossa" matrix and particularly distributed in the central and eastern part of the island. According to [22], these late Pleistocene to Holocene deposits represent the youngest terms and often constitute valley infills.

3. Methodology

The 3D flooding maps along the south-eastern sector of the Lampedusa are based on a double methodological approach: stratigraphic and geomorphological. The stratigraphic reconstruction was carried out through the detailed description of logs and the traditional analysis of depositional outcrops located in some strategic areas (see Section 4).

The geomorphological reconstruction was performed by traditional landscape analysis and the outcrop interpretation was enhanced by the description and interpretation of the Digital Terrain Model (2 m $\times$ 2 m cell-size resolution) of Lampedusa. In particular, some topographic profiles along the south-eastern sector of the island were made using the QGIS Desktop 3.22.8 and Global mapper 18 software and a study of the slopes of the same sector was associated. Finally, using the "3D view" tool it was possible to create base maps for the simulation of homogeneous sea level variations in steps of +5 m, +10 m, and +15 m (see Section 5). Specifically, this tool allows to simulate water sea level changes and/or flooding: to simulate the water coverage/flooding if you increase the water level by some depth over either a fixed single elevation (such as 0 for sea level) or from a selected area feature, such as a flood plain area. For example, with a coastal area selected, one can simulate increasing the sea level by some amount to observe where the water level would reach, taking into account any terrain features that prevent flow, such as levees, buildings in the terrain, etc. (https://www.bluemarblegeo.com/knowledgebase/global-mapper-23/Simulate_Water_Level_Rise_Flooding.htm, accessed on 10 October 2022).

The "Simulate Water Level Rise/Flooding" tool of the Global Mapper software allows to run "Water Rise Calculation" through a dedicated setup command. Specifically, for the creation of our 3D flooding maps, these values were entered as input:

- Water level: 0 m;
- Water level increase amount: 5 m;
- Select what to increase water level from: Sea Level = 0;
- Vertical exaggeration: 5x;
- Resolution with which the terrain is sampled to calculate the flooded area: defaults.

4. Geomorphological Setting of Lampedusa Island

Lampedusa island lies in the central Mediterranean Sea, 35°30′ N latitude, about 250 km south of the Sicilian coasts and 130 km east of those of Tunisia. The island consists of an E–W elongated carbonate shelf, about 11 km long and 3 Km wide, with an area of almost 20 km^2 and a maximum topographic elevation of 134 m a.s.l. reached along its north-western portion (Mt. Albero Sole locality; Figure 6).

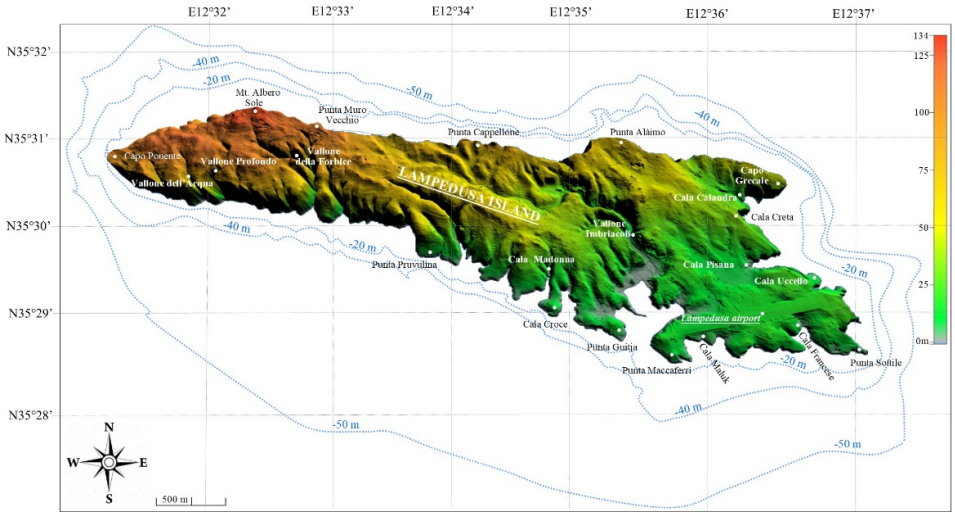

Figure 6. Geomorphological setting of Lampedusa island based on a 2 m × 2 m Digital Terrain Model (https://www.sitr.regione.sicilia.it/geoportale/it/metadata/details/502, accessed on 3 October 2022).

The lithological homogeneity of the island and the sub-horizontal setting of the strata favored the development of a typical tabular morphology deeply incised by several river valleys. In the western part of the island, fluvial canyons exhibit V-shaped sections with approximately 45° dipping flanks. In the eastern part, fluvial valleys are characterized by a flat morphology of the floor (e.g., Vallone Imbriacoli) due to the anthropic reworking of the alluvial deposits for agriculture purposes. The island is characterized by low-lying coasts in the southern and eastern parts, with numerous bays and inlets coinciding with the mouth of valleys cutting the carbonate plateau. Conversely, the northern coast consists of sub-vertical cliffs, up to 120 m high [83,96–98].

Drainage lines exhibit linear or dendritic patterns and the main water courses generally flow towards SSE showing changes in directions from WNW-ESE to NNW-SSE up to north-south.

The quantitative study of the landforms through analysis of the available digital terrain model (2 × 2 m cell-size resolution) into a GIS workstation allowed to derive thematic maps. Statistical slope gradients and slope aspect analysis [98] revealed that the summit topographic surface dips about 7.30° on average toward the N170E direction. This morphological setting suggests that the island has been subjected to differential tilting phases (E–W and N–S) probably related to the regional field deformation [99].

This mechanism, together with the different responses to the erosion of the rocks, has favored the development of coastal landforms, which are characterized by high coasts in the north and west and low-lying coasts in the southeast, respectively.

The northern coastal domain, mainly exposed to waves driven by Mistral wind, exhibits sub-vertical rocky cliffs (Figure 6) with elevations gradually increasing from the east (on average 40–70 m high, Capo Grecale-Punta Alaimo area) to the West (80 to 130 m high, Punta Cappellone-Albero Sole area) in agreement with the orographic setting of the island. High coasts also characterize the western (e.g., Capo Ponente) and southwestern portion of Lampedusa island with sub-vertical cliffs rising up to 100 m a.s.l. Generally, along the entire coastal domain, marine abrasion platforms occur at different elevations suggesting an overall long term uplift of the island.

Moreover, cliffs are often characterized by the absence of modern marine abrasion platforms at their basis. This suggests that these cliffs are almost morphologically stable, although rock fall episodes are quite common along the edge of the main slopes. Morphological denudation drives the cliffs retreat, giving rise to hanging valleys related to the cutoff of drainage systems. The Vallone dell'Acqua and Vallone Profondo in the western part of the island offer typical examples of this phenomenon. Furthermore, numerous karst caves showing a sub-circular shape occur along the cliffs.

The south-eastern area of the island is characterized by rather irregular coastal landforms dominated by alternating high- and low-lying coastal morphologies forming a series of bays and headlands with sandy beaches and cliffs inclined by an average of 45°. Overall, these morphologies describe a rias-type coast (Figure 6), originated by marine ingression in river valleys in response to relative sea level rising or to the subsidence process of the area in response to the tilting events.

5. 3D Flooding Maps

A semi-qualitative study of the impact on the geomorphological setting of Lampedusa island through the analysis of the available digital terrain model (2 × 2 m cell-size resolution; Figure 7) into a GIS workstation allowed to derive 3D flooding maps. Based on the maximum reachable heights and the magnitudes of the earthquakes recorded in the Mediterranean area capable of generating tsunamis (Table 1), we can identify different ranges of reachable runups: 0–5 m, 5–15 m, and >15 m. As mentioned, due to its central position within the Sicilian Channel (Mediterranean Sea), Lampedusa island represents an excellent site to study the geomorphological variations of the landscape following sudden sea level variations connected to seismic events or submarine landslides. The plateau-type morphological setting slightly inclined towards the east (about 1°) is entirely exposed to potential runup waves coming from the south-eastern sector of the island.

Figure 7. Actual geomorphological setting of the south-eastern area of Lampedusa island.

However, the landscape variations of Lampedusa are only described in the south-eastern sector of the island due to the invasion of sea water. In fact, this side of the island is the most vulnerable for two main reasons:

- The main tsunamigenic earthquakes known in the literature are mainly concentrated in the eastern sector of the Mediterranean Sea (Table 1);
- Here, a high concentration of low beaches (on average 5 m high) is present and evolves in the northwest-southeast direction according to a rias coastline (Figure 3).

In the next section, we show 3D flooding maps simulating uniform and coeval water invasion steps of 5 m, 10 m, and 15 m and describe in detail how the morphological setting changes on the island.

5.1. Sea Level Variation: +5 m

The rias morphology of the southern and eastern coastline of the island highlights sectors characterized by very low beaches (named "Cale") alternating with cliffs elongated towards the sea (named "Punte").

Simulating a 5 m runup that uniformly involves this sector of the island, the 3D map (Figure 8) shows that in proximity to Punta Guitgia, Punta Magaianeddu, Punta Manzu, and Punta Pruvulina, the marine invasion does not exceed 20 m landwards. Here, the cliffs are still high enough (about 10 m) and able to shield a runup until 5 m. The marine invasion values decrease (about 10 m) along the eastern coast of Lampedusa: here the cliffs are higher (about 15 m) and more widespread, giving natural protection to the airport area, a strategic point for the island's economy.

Figure 8. 3D flooding map (+5 m) along the southeastern sector of the island of Lampedusa.

In the southern sector, in correspondence to the low beaches of Cala Croce, Cala Madonna, and Cala Galera, an intense invasion marine could reach values of about 100 m. It is noteworthy that the harbor is the most vulnerable area within the southern sector. The harbor area shows submerged areas up to about 300 landwards, although it is protected to the west by Punta Guitgia and to the east by Punta 'O Spada (cliffs up to 10 m high). The southern portion of Vallone Imbriacoli reaches up to 200 m landwards.

The eastern portion of Lampedusa is characterized by high coastlines (above 20 m), but only in correspondence to the Cala Pisana terrestrial areas resulted to be significantly flooded by the sea (up to 120 m).

In conclusion, a 5 m runup wave that homogeneously involves the south-eastern portion of Lampedusa would submerge a total coastal area of about 1 km^2.

5.2. Sea Level Variation: +10 m

With the sea level variation of +10 m (Figure 9), substantial changes in the geomorphological setting of the south-eastern sector of Lampedusa island are evident. Here, the

current height of the cliffs rarely exceeds 10 m; therefore, the marine invasion increases exponentially reaching medium values of about 200 m.

Figure 9. 3D flooding map (+10 m) along the southeastern sector of the island of Lampedusa.

In particular, the morphological setting of the southern coastline is completely distorted, with the preservation of only small portions of paleo cliffs (Punta Guitgia, for example) which are transformed into small islets in the outermost portions. The southern "Cale" are largely submerged or, in the case of deeper incisions, move landward on average 100 m and reach its maximum values along Vallone Imbriacoli, the main paleo incision of the island.

The south-eastern coastline shows a smoother trend than the current one: here, the cliffs are up to 15 m high, preserving a large part of the airport area located in the nearby hinterland. Nevertheless, an increase in the sea level up to +10 m determines the almost total isolation of the airport, which is connected with the rest of the island by a little extended high morphology.

To the east, the highest cliffs of the eastern sector are concentrated and the morphological setting appears roughly unchanged except in the vicinity of Cala Pisana. Here, a 10 m runup can potentially reach distances landwards of about 800 m, bounding the airport area to the north.

In conclusion, a 10 m runup wave that homogeneously involves the south-eastern portion of Lampedusa would submerge a total coastal area of about 3 km^2.

5.3. Sea Level Variation: +15 m

The 3D flooding map with a step +15 m (Figure 10) shows a completely revolutionized morphological setting compared with the current one. In the southern portion, where the cliffs do not exceed 10 m in height, no morphological feature of paleo coastline is preserved. In general, this submerged portion of this sector shows an increase of at least 40% and also the cliffs that protected the airport are submerged. The area occupied by the airport, largely occupied by the sea, is now completely isolated. The harbor and the Lampedusa village are also largely submerged.

In conclusion, a 10 m runup wave that homogeneously involves the south-eastern portion of Lampedusa would submerge a total coastal area of about 9 km^2.

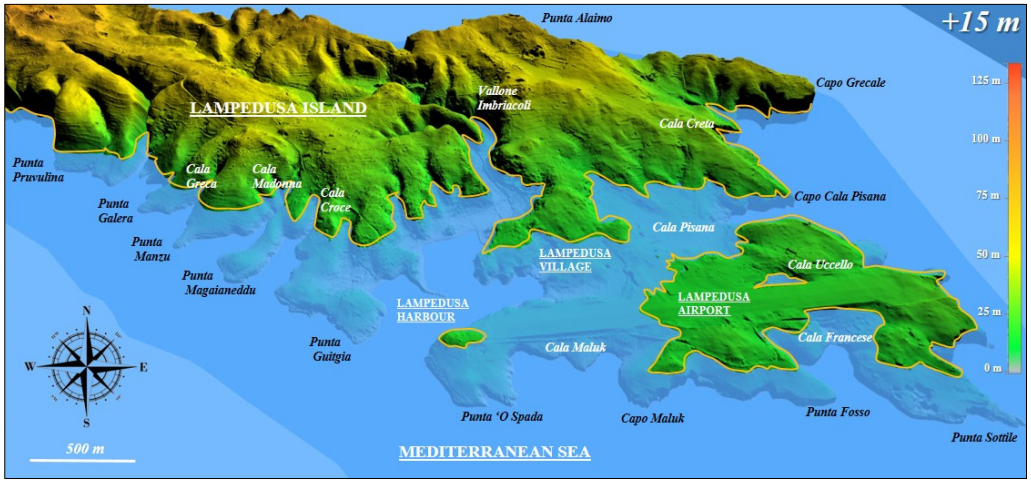

Figure 10. 3D flooding map (+15 m) along the southeastern sector of the island of Lampedusa.

6. Conclusions

The updated stratigraphic analysis of Lampedusa, associated with a detailed study of the geomorphological setting of the island, proved to be a fundamental tool for the evaluation of the tsunami vulnerability of the central area of the Sicilian Channel. The main goals achieved are:

1. The general tabular setting of the Lampedusa island, slightly tilted towards the east, is lithologically associated with medium-low cohesion formations (carbonate mudstones of the Vallone Imbriacoli Unit and marly lithotypes of the Cala Calandra Unit) outcropping in the eastern portion of Lampedusa where the paleo-hydrographic network is well-developed and the coastline is widely low. Therefore, the south-eastern sector of the island appears to be the most suitable for testing the simulations of 3D flooding maps, which was the main goal of this work.
2. The updated stratigraphic analysis of Lampedusa was crucial for a detailed geomorphological reconstruction of the island. On the basis of a high-resolution DEM (2 m × 2 m cells), the 3D flooding maps were carried out assuming three different maximum runup steps (+5 m, +10 m, and + 15 m), comparable with historical tsunamigenic events in the central Mediterranean area.
3. The focal points of Lampedusa (harbor, airport, and main village)—concentrated in the southern sector of the island—already appear threatened with a runup of just +5 m. However, such areas would be seriously compromised with runups of +10 m and +15 m, where the area flooded by the sea grows up to almost 10 times.

Author Contributions: Conceptualization, S.D., L.B. and A.D.S.; methodology, S.D.; software, S.D.; validation, S.D. and A.D.S.; formal analysis, S.D., L.B. and A.D.S.; investigation, S.D. and N.B.; resources, A.D.S.; data curation, S.D. and N.B.; writing—original draft preparation, S.D., L.B. and S.U.; writing—review and editing, S.D. and A.D.S.; visualization, V.B., N.M.D. and S.U.; supervision, A.D.S.; funding acquisition, A.D.S. All authors have read and agreed to the published version of the manuscript.

Funding: This research was funded by the Interreg Italy-Malta SIMIT THARSY Project—CUP G72D18000050006.

Institutional Review Board Statement: Not applicable.

Informed Consent Statement: Not applicable.

Data Availability Statement: Euro-Mediterranean Tsunami Catalogue—EMTC: https://ingv.maps.arcgis.com/apps/webappviewer/index.html?id=a14231712588470ea1c4454301b8294c&showLayers=EMTC%202.0, accessed on 3 October 2022; Digital Terrain Model 2 m × 2 m: https://www.sitr.regione.sicilia.it/geoportale/it/metadata/details/502, accessed on 3 October 2022.

Acknowledgments: The authors wish to thank the Special Issue editors and four anonymous reviewers for their constructive comments that helped to significantly improve the manuscript.

Conflicts of Interest: The authors declare no conflict of interest.

References

1. Intergovernmental Oceanographic Commission of UNESCO. Reducing and Managing the Risk of Tsunamis. In *IOC Manuals and Guides, 57*; IOC/2011/MG/57Rev.2; UNESCO: Paris, France, 2011; p. 74.
2. D'Acremont, E.; Lafuerza, S.; Rabaute, A.; Lafosse, M.; Jollivet Castelot, M.; Gorini, C.; Alonso, B.; Ercilla, G.; Vazquez, J.T.; Vandorpe, T.; et al. Distribution and origin of submarine landslides in the active margin of the southern Alboran Sea (Western Mediterranean Sea). *Mar. Geol.* **2022**, *445*, 106739. [CrossRef]
3. Zaniboni, F.; Pagnoni, G.; Paparo, M.A.; Gauchery, T.; Rovere, M.; Argnani, A.; Armigliato, A.; Tinti, S. Tsunamis from submarine collapses along the eastern slope of the Gela basin (Strait of Sicily). *Front. Earth Sci.* **2021**, *8*, 602171. [CrossRef]
4. Valensise, G.; Pantosti, D.A. 125 Kyr-long geological record of seismic source repeatability: The Messina Straits (southern Italy) and the 1908 earthquake (Ms 7 1/2). *Terra Nova* **1992**, *4*, 472–483. [CrossRef]
5. Okal, E.A.; Synolakis, C.E.; Uslu, B.; Kalligeris, N.; Voukouvalas, E. The 1956 earthquake and tsunami in Amorgos, Greece. *Geophys. J. Int.* **2009**, *178*, 1533–1554. [CrossRef]
6. Alasset, P.J.; Hébert, H.; Maouche, S.; Calbini, V.; Meghraoui, M. The tsunami induced by the 2003 Zemmouri earthquake (MW = 6.9, Algeria): Modelling and results. *Geophys. J. Int.* **2006**, *166*, 213–226. [CrossRef]
7. Cattaneo, A.; Babonneau, N.; Ratzov, G.; Yelles, K.; Brac, R. Searching for the seafloor signature of the 21 May 2003 Boumerdes earthquake offshore central Algeria. *Nat. Hazards Earth Syst. Sci.* **2012**, *12*, 2159–2172. [CrossRef]
8. Samaras, A.G.; Karambas, T.V.; Archetti, R. Simulation of tsunami generation, propagation and coastal inundation in the Eastern Mediterranean. *Ocean. Sci.* **2015**, *11*, 643–655. [CrossRef]
9. Scicchitano, G.; Costa, B.; Di Stefano, A.; Longhitano, S.G.; Monaco, C. Tsunami and storm deposits preserved within a ria-type rocky coastal setting (Siracusa, SE Sicily). *Z. Geomorphol. Suppl.* **2010**, *54*, 51. [CrossRef]
10. Lo Re, C.; Manno, G.; Ciraolo, G. Tsunami propagation and flooding in Sicilian Coastal Areas by means of a weakly dispersive Boussinesq model. *Water* **2020**, *12*, 1448. [CrossRef]
11. Paparo, M.A.; Armigliato, A.; Pagnoni, G.; Zaniboni, F.; Tinti, S. Earthquake-triggered landslides along the Hyblean-Malta Escarpment (off Augusta, eastern Sicily, Italy)–assessment of the related tsunamigenic potential. *Adv. Geosci.* **2017**, *44*, 1–8. [CrossRef]
12. Milia, A.; Iannace, P.; Torrente, M.M. Active tectonic structures and submarine landslides offshore southern Apulia (Italy): A new scenario for the 1743 earthquake and subsequent tsunami. *Geo-Mar. Lett.* **2017**, *37*, 229–239. [CrossRef]
13. Evelpidou, N.; Karkani, A.; Polidorou, M.; Saitis, G.; Zerefos, C.; Synolakis, C.; Gogou, M. Palaeo-Tsunami Events on the Coasts of Cyprus. *Geosciences* **2022**, *12*, 58. [CrossRef]
14. Biolchi, S.; Furlani, S.; Antonioli, F.; Baldassini, N.; Causon Deguara, J.; Devoto, S.; Scicchitano, G. Boulder accumulations related to extreme wave events on the eastern coast of Malta. *Nat. Hazards Earth Sys.* **2016**, *16*, 737–756. [CrossRef]
15. Evelpidou, N.; Zerefos, C.; Synolakis, C.; Repapis, C.; Karkani, A.; Polidorou, M.; Saitis, G. Coastal Boulders on the SE Coasts of Cyprus as Evidence of Palaeo-Tsunami Events. *J. Mar. Sci. Eng.* **2020**, *8*, 812. [CrossRef]
16. Papathoma, M.; Dominey-Howes, D. Tsunami vulnerability assessment and its implications for coastal hazard analysis and disaster management planning, Gulf of Corinth, Greece. *Nat. Hazards Earth Syst. Sci.* **2003**, *3*, 733–747. [CrossRef]
17. Ambraseys, N.; Synolakis, C. Tsunami catalogs for the Eastern Mediterranean, revisited. *J. Earthq. Eng.* **2010**, *14*, 309–330. [CrossRef]
18. Dominey-Howes, D.; Papathoma, M. Validating a tsunami vulnerability assessment model (the PTVA model) using field data from the 2004 Indian Ocean tsunami. *Nat. Hazards* **2007**, *40*, 113–136. [CrossRef]
19. Sørensen, M.B.; Spada, M.; Babeyko, A.; Wiemer, S.; Grünthal, G. Probabilistic tsunami hazard in the Mediterranean Sea. *J. Geophys. Res.* **2012**, *117*, 1–15. [CrossRef]
20. Batzakis, D.V.; Misthos, L.M.; Voulgaris, G.; Tsanakas, K.; Andreou, M.; Tsodoulos, I.; Karymbalis, E. Assessment of Building Vulnerability to Tsunami Hazard in Kamari (Santorini Island, Greece). *J. Mar. Sci. Eng.* **2020**, *8*, 886. [CrossRef]
21. Dominey-Howes, D. Assessment of tsunami magnitude and implications for urban hazard planning. *Disaster Prev. Manag.* **1998**, *7*, 176–182. [CrossRef]
22. Grasso, M.; Pedley, H.M. The Pelagian Islands: A new geological interpretation from sedimentological and tectonic studies and its bearing on the evolution of the Central Mediterranean Sea (Pelagian Block). *Geol. Romana* **1985**, *24*, 13–34.
23. Distefano, S.; Gamberi, F.; Baldassini, N.; Di Stefano, A. Late Miocene to Quaternary structural evolution of the Lampedusa Island offshore. *Geogr. Fis. Din. Quat.* **2018**, *41*, 17–31.
24. Distefano, S.; Gamberi, F.; Baldassini, N.; Di Stefano, A. Neogene stratigraphic evolution of a tectonically controlled continental shelf: The example of the Lampedusa Island. *Ital. J. Geosci.* **2019**, *138*, 418–431. [CrossRef]
25. Distefano, S.; Gamberi, F.; Borzì, L.; Di Stefano, A. Quaternary Coastal Landscape Evolution and Sea-Level Rise: An Example from South-East Sicily. *Geosciences* **2021**, *11*, 506. [CrossRef]

26. Distefano, S.; Gamberi, F.; Baldassini, N.; Di Stefano, A. Quaternary evolution of coastal plain in response to sea-level changes: Example from south-east Sicily (Southern Italy). *Water* **2021**, *13*, 1524. [CrossRef]
27. Borzì, L.; Anfuso, G.; Manno, G.; Distefano, S.; Urso, S.; Chiarella, D.; Di Stefano, A. Shoreline Evolution and Environmental Changes at the NW Area of the Gulf of Gela (Sicily, Italy). *Land* **2021**, *10*, 1034. [CrossRef]
28. Lorito, S.; Tiberti, M.M.; Basili, R.; Piatanesi, A.; Valensise, G. Earthquake-generated tsunamis in the Mediterranean Sea: Scenarios of potential threats to southern Italy. *J. Geophys. Res.* **2008**, *113*. [CrossRef]
29. Tinti, S.; Armigliato, A.; Manucci, A.; Pagnoni, G.; Zaniboni, F.; Yalçiner, A.C.; Altinok, Y. The generating mechanisms of the August 17, 1999 Izmit bay (Turkey) tsunami: Regional (tectonic) and local (mass instabilities) causes. *Mar. Geol.* **2006**, *225*, 311–330. [CrossRef]
30. Pareschi, M.T.; Boschi, E.; Mazzarini, F.; Favalli, M. Large submarine landslides offshore Mt. Etna. *Geoph. Res. Lett.* **2006**, *33*. [CrossRef]
31. Maramai, A.; Graziani, L.; Brizuela, B. Italian Tsunami Effects Database (ITED): The first database of tsunami effects observed along the Italian coasts. *Nat. Hazards Earth Syst. Sci. Discuss.* **2019**, *9*, 596044. [CrossRef]
32. Barbano, M.S.; Pirrotta, C.; Gerardi, F. Large boulders along the south-eastern Ionian coast of Sicily: Storm or tsunami deposits? *Mar. Geol.* **2010**, *275*, 140–154. [CrossRef]
33. Gerardi, F.; Smedile, A.; Pirrotta, C.; Barbano, M.S.; De Martini, P.M.; Pinzi, S.; Troja, S.O. Geological record of tsunami inundations in Pantano Morghella (south-eastern Sicily) both from near and far-field sources. *Nat. Hazards Earth Syst. Sci.* **2012**, *12*, 1185–1200. [CrossRef]
34. Pararas-Carayannis, G. The earthquake and tsunami of July 21, 365 AD in the Eastern Mediterranean Sea-Review of Impact on the Ancient World-Assessment of recurrence and future impact. *Sci. Tsunami Hazards* **2011**, *30*, 253–292.
35. Kelly, G. Ammianus and the great tsunami. *J. Rom. Stud.* **2004**, *94*, 141–167. [CrossRef]
36. Graziani, L.; Maramai, A.; Tinti, S. A revision of the 1783–1784 Calabrian (southern Italy) tsunamis. *Nat. Hazards Earth Syst. Sci.* **2006**, *6*, 1053–1060. [CrossRef]
37. Guidoboni, E.; Ferrari, G.; Mariotti, D.; Comastri, A.; Tarabusi, G.; Sgattoni, G.; Valensise, G. *CFTI5Med, Catalogo dei Forti Terremoti in Italia (461 aC-1997) e nell'area Mediterranea (760 aC-1500)*; Istituto Nazionale di Geofisica e Vulcanologia (INGV): Rome, Italy, 2018.
38. Ambraseys, N.N. Data for the investigation of the seismic sea-waves in the Eastern Mediterranean. *Bull. Seismol. Soc. Am.* **1962**, *52*, 895–913.
39. Papadopoulos, G.A.; Chalkis, B.J. Tsunamis observed in Greece and the surrounding area from antiquity up to the present times. *Mar. Geol.* **1984**, *56*, 309–317. [CrossRef]
40. Papadopoulos, G.A.; Vassilopoulou, A. Historical and archaeological evidence of earthquakes and tsunamis felt in the Kythira strait, Greece. In *Tsunami Research at the End of a Critical Decade*; Springer: Dordrecht, The Netherlands, 2001; pp. 119–138.
41. Platania, G. *Il Maremoto Dello Stretto di Messina del 28 Dicembre 1908*; Modena (Italy); Societá Tipografica Modenese: Rome, Italy, 1909; pp. 1–92.
42. Platania, G. I fenomeni marittimi che accompagnarono il terremoto di Messina del 28 dicembre 1908. *Riv. Geogr. Ital.* **1909**, *16*, 154–161.
43. Baratta, M. *La Catastrofe Sismica Calabro Messinese (28 Dicembre 1908)*; Presso la Società Geografica Italiana: Rome, Italy, 1910.
44. Maramai, A.; Graziani, L.; Tinti, S. Tsunamis in the Aeolian Islands (southern Italy): A review. *Mar. Geol.* **2005**, *215*, 11–21. [CrossRef]
45. Ambraseys, N.N. The seismic sea wave of July 9, 1956, in the Greek Archipelago. *J. Geoph. Res.* **1960**, *65*, 1257–1265. [CrossRef]
46. Tinti, S.; Maramai, A.; Graziani, L. The new catalogue of Italian tsunamis. *Nat. Hazards* **2004**, *33*, 439–465. [CrossRef]
47. Piatanesi, A.; Tinti, S. A revision of the 1693 eastern Sicily earthquake and tsunami. *J. Geophys. Res. Solid Earth* **1998**, *103*, 2749–2758. [CrossRef]
48. Bianca, M.; Monaco, C.; Tortorici, L.; Cernobori, L. Quaternary normal faulting in southeastern Sicily (Italy): A seismic source for the 1693 large earthquake. *Geophys. J. Int.* **1999**, *139*, 370–394. [CrossRef]
49. Monaco, C.; Tortorici, L. Active faulting in the Calabrian arc and eastern Sicily. *J. Geodyn.* **2000**, *29*, 407–424. [CrossRef]
50. Azzaro, R.; Barbano, M.S. Analysis of the seismicity of Southeastern Sicily: A proposed tectonic interpretation. *Ann. Geophys.* **2000**, *43*, 172–188. [CrossRef]
51. Civile, D.; Lodolo, E.; Tortorici, L.; Lanzafame, G.; Brancolini, G. Relationships between magmatism and tectonics in a continental rift: The Pantelleria Island region (Sicily Channel, Italy). *Mar. Geol.* **2008**, *251*, 32–46. [CrossRef]
52. Vött, A.; Bareth, G.; Brückner, H.; Curdt, C.; Fountoulis, I.; Grapmayer, R.; Willershäuser, T. Beachrock-type calcarenitic tsunamites along the shores of the eastern Ionian Sea (western Greece)-case studies from Akarnania, the Ionian Islands and the western Peloponnese. *Z. Geomorphol. Suppl.* **2010**, *54*, 1. [CrossRef]
53. Mastronuzzi, G.; Calcagnile, L.; Pignatelli, C.; Quarta, G.; Stamatopoulos, L.; Venisti, N. Late Holocene tsunamogenic coseismic uplift in Kerkira Island, Greece. *Quat. Int.* **2014**, *332*, 48–60. [CrossRef]
54. Mastronuzzi, G. Tsunami in Mediterranean sea. *Egypt. J. Environ. Chang.* **2010**, *2*, 1–12.
55. Pirazzoli, P.A.; Stiros, S.C.; Arnold, M.; Laborel, J.; Laborel-Deguen, F. Late Holocene coseismic vertical displacements and tsunami deposits near Kynos, Gulf of Euboea, Central Greece. *Phys. Chem. Earth* **1999**, *24*, 361–367. [CrossRef]

56. Mastronuzzi, G.; Sansò, P. Boulders transport by catastrophic waves along the Ionian coast of Apulia (southern Italy). *Mar. Geol.* **2000**, *170*, 93–103. [CrossRef]
57. Gianfreda, F.; Mastronuzzi, G.; Sansò, P. Impact of historical tsunamis on a sandy coastal barrier: An example from the northern Gargano coast, southern Italy. *Nat. Hazards Earth Syst.* **2001**, *1*, 213–219. [CrossRef]
58. Kelletat, D.; Schellmann, G. Tsunamis on Cyprus: Field evidences and 14C dating results. *Z. Geomorphol.* **2002**, *46*, 19–34. [CrossRef]
59. Whelan, F.; Kelletat, D. Geomorphic evidence and relative and absolute dating results for tsunami events on Cyprus. *Sci. Tsunami Hazards* **2002**, *20*, 3–18.
60. Wang, Y.; Heidarzadeh, M.; Satake, K.; Mulia, I.E.; Yamada, M. A tsunami warning system based on offshore bottom pressure gauges and data assimilation for Crete Island in the Eastern Mediterranean Basin. *J. Geophys. Res.-Solid Earth* **2020**, *125*, e2020JB020293. [CrossRef]
61. Heidarzadeh, M.; Wang, Y.; Satake, K.; Mulia, I.E. Potential deployment of offshore bottom pressure gauges and adoption of data assimilation for tsunami warning system in the western Mediterranean Sea. *Geosci. Lett.* **2019**, *6*, 19. [CrossRef]
62. Pino, N.A.; Piatanesi, A.; Valensise, G.; Boschi, E. The 28 December 1908 Messina Straits earthquake (Mw 7.1): A great earthquake throughout a century of seismology. *Seismol. Res. Lett.* **2009**, *80*, 243–259. [CrossRef]
63. Guidoboni, E.; Mariotti, D. Il terremoto e il maremoto del 1908: Effetti e parametri sismici. In *Il Terremoto e il Maremoto del 28 Dicembre 1908: Analisi Sismologica, Impatto, Prospettive*; Dipartimento della Protezione Civile, Istituto Nazionale di Geofisica e Vulcanologia: Rome, Italy, 2008.
64. Tinti, S.; Armigliato, A.; Pagnoni, G.; Zaniboni, F. Scenarios of giant tsunamis of tectonic origin in the Mediterranean. *ISET J. Earthq. Technol.* **2005**, *42*, 171–188.
65. Papadopoulos, G. *Tsunamis in the European-Mediterranean Region: From Historical Record to Risk Mitigation*; Elsevier: Amsterdam, The Netherlands, 2015.
66. Soloviev, S.L.; Solovieva, O.N.; Go, C.N.; Kim, K.S.; Shchetnikov, N.A. *Tsunamis in the Mediterranean Sea 2000 BC-2000 AD (Vol. 13)*; Springer Science & Business Media: Berlin/Heidelberg, Germany, 2000.
67. Paris, R.; Wassmer, P.; Sartohadi, J.; Lavigne, F.; Barthomeuf, B.; Desgages, E.; Gomez, C. Tsunamis as geomorphic crises: Lessons from the December 26, 2004 tsunami in Lhok Nga, west Banda Aceh (Sumatra, Indonesia). *Geomorphology* **2009**, *104*, 59–72. [CrossRef]
68. Luque, L.; Lario, J.; Civis, J.; Silva, P.G.; Zazo, C.; Goy, J.L.; Dabrio, C.J. Sedimentary record of a tsunami during Roman times, Bay of Cadiz, Spain. *J. Quat. Sci. Publ. Quat. Res. Assoc.* **2002**, *17*, 623–631. [CrossRef]
69. Paris, R.; Fournier, J.; Poizot, E.; Etienne, S.; Morin, J.; Lavigne, F.; Wassmer, P. Boulder and fine sediment transport and deposition by the 2004 tsunami in Lhok Nga (western Banda Aceh, Sumatra, Indonesia): A coupled offshore-onshore model. *Mar. Geol.* **2010**, *268*, 43–54. [CrossRef]
70. Hollenstein, C.; Kahle, H.G.; Geiger, A.; Jenny, S.; Goes, S.; Giardini, D. New GPS constraints on the Africa-Eurasia plate boundary zone in southern Italy. *Geoph. Res. Lett.* **2003**, *30*. [CrossRef]
71. D'Agostino, N.; Selvaggi, G. Crustal motion along the Eurasia-Nubia plate boundary in the Calabrian Arc and Sicily and active extension in the Messina Straits from GPS measurements. *J. Geophis. Res. Solid Earth* **2004**, *109*. [CrossRef]
72. Serpelloni, E.; Vannucci, G.; Pondrelli, S.; Argnani, A.; Casula, G.; Anzidei, M.; Gasperini, P. Kinematics of the Western Africa-Eurasia plate boundary from focal mechanisms and GPS data. *Geophys. J. Int.* **2007**, *169*, 1180–1200. [CrossRef]
73. Catalano, S.; De Guidi, G.; Monaco, C.; Tortorici, G.; Tortorici, L. Active faulting and seismicity along the Siculo–Calabrian Rift Zone (southern Italy). *Tectonophysics* **2008**, *453*, 177–192. [CrossRef]
74. Antonelli, M.; Franciosi, R.; Pezzi, G.; Querci, A.; Ronco, G.P.; Vezzani, F. Paleogeographic evolution and structural setting of the northern side of the Sicily Channel. *Mem. Della Soc. Geol. Ital.* **1988**, *41*, 141–157.
75. Argnani, A. The Strait of Sicily rift zone: Foreland deformation related to the evolution of a back-arc basin. *J. Geodyn.* **1990**, *12*, 311–331. [CrossRef]
76. Reuther, C.D.; Eisbacher, G.H. Pantelleria Rift—Crustal extension in a convergent intraplate setting. *Geol. Rundsch.* **1985**, *74*, 585–597. [CrossRef]
77. Grasso, M.; Butler, R.W.H.; La Manna, F. *Thin skinned deformation and structural evolution in the NE segment of the Gela Nappe, SE Sicily*; Università di Camerino: Camerino, Italy, 1990; pp. 9–17.
78. Finetti, I. Geophysical study of the Sicily Channel rift zone. *Boll. Geofis. Teor. Appl.* **1984**, *26*, 101–102.
79. Boccaletti, M.; Cello, G.; Tortorici, L. Transtensional tectonics in the Sicily Channel. *J. Struct. Geol.* **1987**, *9*, 869–876. [CrossRef]
80. Torelli, L.; Grasso, M.; Mazzoldi, G.; Peis, D.; Gori, D. Cretaceous to Neogene structural evolution of the Lampedusa shelf (Pelagian Sea, Central Mediterranean). *Terra Nova* **1995**, *7*, 200–212. [CrossRef]
81. Burollet, P.F.; Mugniot, J.M.; Sweeney, P. The geology of the Pelagian block: The margins and basins off southern Tunisia and Tripolitania. In *The Ocean Basins and Margins*; Springer: Boston, MA, USA, 1978; pp. 331–359.
82. Winnock, E. *Structure du Bloc Pélagien*; Consiglio Nazionale Delle Ricerche: Rome, Italy, 1981; pp. 445–464.
83. Giraudi, C. The upper Pleistocene to Holocene sediments on the Mediterranean island of Lampedusa (Italy). *J. Quat. Sci.* **2004**, *19*, 537–545. [CrossRef]
84. Distefano, S.; Gamberi, F.; Di Stefano, A. Stratigraphic and structural reconstruction of an offshore sector of the Hyblean Foreland ramp (southern Italy). *Ital. J. Geosc.* **2019**, *138*, 390–403. [CrossRef]

85. Maniscalco, R.; Casciano, C.I.; Distefano, S.; Grossi, F.; Di Stefano, A. Facies analysis in the Second Cycle Messinian evaporites predating the early Pliocene reflooding: The Balza Soletta section (Corvillo Basin, central Sicily). *Ital. J. Geosci.* **2019**, *138*, 301–316. [CrossRef]
86. Fabbrini, A.; Baldassini, N.; Caricchi, C.; Foresi, L.M.; Sagnotti, L.; Dinarès-Turell, J.; Di Stefano, A.; Lirer, F.; Menichetti, M.; Winkler, A.; et al. In search of the Burdigalian GSSP: New evidence from the Contessa Section (Italy). *Ital. J. Geosci.* **2019**, *138*, 274–295. [CrossRef]
87. Colantoni, P. Note di geologia marina sul Canale di Sicilia. *G. Geol.* **1975**, *40*, 181–207.
88. Boccaletti, M.; Nicolich, R.; Tortorici, L. The Calabrian Arc and the Ionian Sea in the dynamic evolution of the Central Mediterranean. *Mar. Geol.* **1984**, *55*, 219–245. [CrossRef]
89. Ben-Avraham, Z.; Grasso, M. Collisional zone segmentation in Sicily and surrounding areas in the Central Mediterranean. *Ann. Tecton.* **1990**, *4*, 131–139.
90. Gardiner, W.; Grasso, M.; Sedgeley, D. Plio-Pleistocene fault movement as evidence for mega-block kinematics within the Hyblean—Malta Plateau, Central Mediterranean. *J. Geodyn.* **1995**, *19*, 35–51. [CrossRef]
91. Tavarnelli, E.; Prosser, G. The complete Apennines orogenic cycle preserved in a transient single outcrop near San Fele, Lucania, Southern Italy. *J. Geol. Soc.* **2003**, *160*, 429–434. [CrossRef]
92. Finetti, I.R.; Del Ben, A. Crustal tectono-stratigraphic setting of the Adriatic Sea from new CROP seismic data. In *CROP, Deep Seismic Exploration of the Mediterranean Region*; Elsevier: Amsterdam, The Netherlands, 2005; pp. 519–547.
93. Finetti, I.R. *CROP Project: Deep Seismic Exploration of the Central Mediterranean and Italy*; Elsevier: Amsterdam, The Netherlands, 2005.
94. Grasso, M.; Torelli, L.; Mazzoldi, G. Cretaceous—Palaeogene sedimentation patterns and structural evolution of the Tunisian shelf, offshore the Pelagian islands (central Mediterranean). *Tectonophysics* **1999**, *315*, 235–250. [CrossRef]
95. Segre, G. *Biogeografia delle Isole Pelagie*; Rendiconti Accademia Nazionale dei Lincei: Rome, Italy, 1960; Volume 11, pp. 115–162.
96. Grasso, M.; Pedley, H.M. The sedimentology and development of Terravecchia Formation carbonates (Upper Miocene) of North Central Sicily: Possible eustatic influence on facies development. *Sediment. Geol.* **1988**, *57*, 131–149. [CrossRef]
97. Buccheri, G.; Renda, P.; Morreale, C.; Sorrentino, G. Il Tirreniano dell'Isola di Lampedusa (Arcipelago Pelagiano, Agrigento, Italia): Le successioni di Cala Maluk e Cala Uccello. *Boll. Soc. Geol. Ital.* **1999**, *118*, 361–373.
98. Panzera, F.; Lombardo, G.; Sicali, S.; D'Amico, S. Surface geology and morphologic effects on seismic site response: The study case of Lampedusa, Italy. *Phys. Chem. Earth* **2017**, *98*, 62–72. [CrossRef]
99. Meccariello, M.; Ferranti, L.; Barreca, G.; Palano, M. New insights on the tectonics of the Lampedusa Plateau from the integration of offshore, on-land and space geodetic data. *Ital. J. Geosc.* **2017**, *136*, 206–219. [CrossRef]